Asociación Argentina
de Mecánica Computacional

Mecánica Computacional Vol XXVIII, págs. 3251-3264 (artículo completo)
Cristian García Bauza, Pablo Lotito, Lisandro Parente, Marcelo Vénere (Eds.)
Tandil, Argentina, 3-6 Noviembre 2009

MULTI-DOMAIN MODEL FOR FAULT DIAGNOSIS ON ELECTRIC TRACTION DRIVES USING BOND GRAPHS

Luis I. Silva, Pablo M. de la Barrera, Cristian H. De Angelo, Guillermo R. Bossio and Guillermo O. García

Grupo de Electrónica Aplicada, Universidad Nacional de Río Cuarto, Ruta Nac. #36 Km. 601, X5804BYA Río Cuarto, Córdoba, Argentina, lsilva@ing.unrc.edu.ar

Keywords: Modeling, Simulation, Bond-Graph, Induction Motor Dynamics.

Abstract. In this work a dynamic model of the induction machine that considers the thermal behavior is developed using Bond Graphs (BG). The thermal model is based on considering the slots and teeth as independent elements with their own temperature. It corresponds to a real motor used in the tractive wheel of an electric vehicle. The model of the vehicle is also obtained in BG and is coupled to the motor. The complete model allows simulating the whole dynamics in a single model and the analysis of electrical/mechanical/thermal interaction is performed. Simulation results are intended to illustrate this interaction under faulty and healthy conditions in the stator winding. The impact on the mechanical and thermal domain produced by a fault in the electrical domain is analyzed.

1 INTRODUCTION

The advent of new power electronic components and microcontrollers produced a change in the type of motor used for variable speed applications. Aforetime they were implemented with DC machines but nowadays the AC machine is the most used due to weight, maintenance and economical advantages, among others. However, the vast complexity of the working principle calls for the development of field oriented control (FOC) strategies (Krishnan, 2001) that are based on the dynamic model.

The conventional model of induction machine (IM) in *dq0* variables (Krause et al., 1994) is widely used to tune digital controllers used in FOC. With few modifications it is possible to consider other phenomena such as: iron losses (IL) and/or additional losses ("*stray load losses*") (Lamine and Levi, 2004); faults concerning stator winding short-circuits (Tallam et al., 2002) and broken rotor bars (Bellini et al., 2006).

In García (1994) a model in *dq0* variables that considers IL is presented. Based on this model it is possible to derive new control schemes capable to avoid errors in the estimation of flux and torque (needed in the FOC) when IL appear (García et al., 1994; Levi, 1995; Levi et al., 1996; de la Barrera et al., 2008). Even more, since motors drive mechanical loads, the control performance analysis needs unavoidably an accurate model of the mechanical system coupled.

When this "Motor - Load" system is working, the own thermal characteristics plus the environment interaction determine the working temperature. In the case under study, the motor is used to drive an electric vehicle and the ventilation (important part of the environment interaction) is function of the vehicle's velocity. Due to the negative impact of overheating on the motor life, it is important to study the thermal behavior during the design stage. Because of this fact, the development of modeling methods capable to reproduce the electric as well as the thermal and mechanical behavior becomes essential. Using these models it is feasible to do the thermal analysis together with the evaluation of: fault detection systems, performance of different controllers, configurations, topologies and materials applied on the motor. This complete analysis can be carried out even prior to the actual construction.

Bond Graph (BG) modeling is best suited to model large scale physical systems independently of their nature (Cellier, 1991; Karnopp et al., 2000). That is why this tool becomes fundamental for modeling multi-domain systems in general and the electrical/mechanical/thermal nature of the IM in particular.

This work represents a continuation of that presented in (Silva et al., 2009). The relative improvements respect to the model firstly presented are: the stator resistances are in the *abc* frame. It allows a temperature distribution analysis of the stator and the inclusion of faults associated to stator winding. On the other hand, the rest of the electric dynamics is modeled in the *dq0* frame. The electric variables expressed in this frame are needed to implement FOC. Secondly, the thermal model that takes into account the spatial distribution of the stator winding is constructed. Finally, the mechanical model (in the previous work composed by a rotating inertia with viscosity friction and external load torque) was replaced by the longitudinal dynamical model of the electric vehicle is where the motor is really placed. The last step consists on the integration of these sub-systems into a complete dynamical model that is used to perform different simulations.

The rest of the paper is organized as follows: In section 2 the electric model of the IM is presented. Section 3 is devoted to describe and model the thermal and mechanical behavior. Along section 4 the integration of the sub-systems is carried out. Section 5 shows simulation results of the complete system performance. In section 6 conclusions about the benefits of the

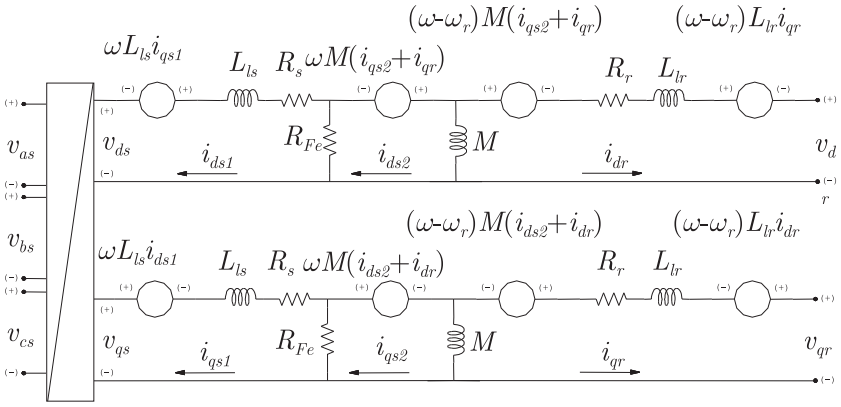

Figure 1: IM equivalent circuit in *dq0* variables.

model are provided together with future works.

2 IM ELECTRIC MODEL

In this section a dynamic model of the IM in *dq0* variables considering IL is presented. The stator IL is represented by an equivalent resistance (R_{Fe}) in parallel with the magnetizing branch. Fig. 1 shows the equivalent circuit in *dq0* variables. The model does not consider variables in the *0* axis because it is balanced and the neutral conductor is not connected.

2.1 Electrical Model Considering Iron Losses

Based on the circuit in Fig. 1, the voltage and flux equations are deduced by inspection:

$$\begin{aligned}
v_{ds} &= -\omega\lambda_{qs1} + \dot{\lambda}_{ds1} + R_s i_{ds1} + R_{Fe}\left(i_{ds1} - i_{ds2}\right) \\
v_{qs} &= \omega\lambda_{ds1} + \dot{\lambda}_{qs1} + R_s i_{qs1} + R_{Fe}\left(i_{qs1} - i_{qs2}\right) \\
0 &= -\omega\lambda_{qm} + \dot{\lambda}_{dm} + R_{Fe}\left(i_{ds2} - i_{ds1}\right) \\
0 &= \omega\lambda_{dm} + \dot{\lambda}_{qm} + R_{Fe}\left(i_{qs2} - i_{qs1}\right) \\
v_{dr} &= \left(\omega - \omega_r\right)\left(\lambda_{qr1} + \lambda_{qm}\right) + \left(\dot{\lambda}_{dr1} + \dot{\lambda}_{dm}\right) + R_r i_{dr} \\
v_{qr} &= \left(\omega - \omega_r\right)\left(\lambda_{dr1} + \lambda_{dm}\right) + \left(\dot{\lambda}_{qr1} + \dot{\lambda}_{qm}\right) + R_r i_{qr}
\end{aligned} \tag{1}$$

where the currents, fluxes and voltages are represented by i, λ and v, respectively; subscripts q and d indicate variables referred to those axes, and s, r and m refer to stator, rotor and air-gap, respectively.

The stator, rotor and air-gap fluxes equations are:

$$\begin{aligned}
\lambda_{ds1} &= L_{ls} i_{ds1} \\
\lambda_{qs1} &= L_{ls} i_{qs1} \\
\lambda_{dm} &= M(i_{ds2} + i_{dr}) \\
\lambda_{qm} &= M(i_{qs2} + i_{qr}) \\
\lambda_{dr1} &= L_{lr} i_{dr} \\
\lambda_{qr1} &= L_{lr} i_{qr}
\end{aligned} \tag{2}$$

Applying power invariant transformation, the electromagnetic torque can be expressed in

dq0 variables as (Krause et al., 1994):

$$T_e = \left(\frac{P}{2}\right) M \left(i_{qs2}\, i_{dr} - i_{ds2}\, i_{qr}\right) \tag{3}$$

where P is the number of poles. From (2) and (3) can be obtained an alternative expression of T_e that is useful in the BG model:

$$T_e = \left(\frac{P}{2}\right) \left(i_{dr}\lambda_{qm} - i_{qr}\lambda_{dm}\right) \tag{4}$$

2.2 Electric Model in Bond Graph

To design and test different control strategies it is necessary to have an accurate electrical model of the IM as well as the mechanical load. Taking into account that using BG it is possible to acquire a model of both domains, many efforts were made to represent the electrical dynamics of the IM using this formalism (Junco, 1999; Karnopp, 2003).

Two novel approaches are included in the model respect to those developed in current literature:

1. Stator resistances are represented as a series of twelve modulated resistive sources "**RS**" in the *abc* frame.

2. Modulated gyrators "**MGY**" are used to represent the virtual voltage sources included when the electric variables are refered in the *dq0* frame (Donaire, 2009).

Fig. 2.a shows these ideas in the standard formalism used to represent electric circuits while Fig. 2.b shows the equivalent model in BG. Here **K** and $\mathbf{K}^{\mathbf{T}}$ are the matrices that represent the power invariant transformation from *abc* to *dq0* and from *dq0* to *abc*, respectively (Krause et al., 1994).

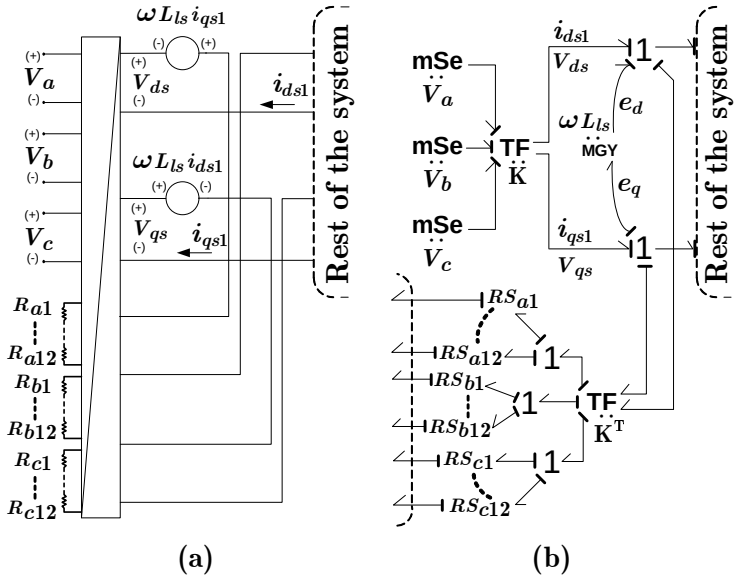

Figure 2: a) Standard electric circuit. b) Equivalent circuit in BG.

The approach proposed in 1) is useful for modeling the spatial distribution of the stator winding resistances. The primary bond of the "**RS**" belongs to the electric domain while the

secondary bond lies in the thermal domain. This concept is explained in detail along next section. It is important to bear in mind that in the *dq0* "side" this three resistances (R_a, R_b and R_c) are seen as the two statoric resistances used in the standard IM model (in *dq0* variables).

The approach in 2) illustrates in a more comprehensible manner the power conservation. This is derived from (Donaire, 2009) but here it was extended in order to adapt this idea to the model that considers IL. Next, the analysis of the two virtual voltage sources in the left side of Fig. 1 is performed. The subscript *d* is used for the upper bond of the "**MGY**" and *q* is used for the lower one (Fig. 2.b).

The relationship in the **MGY** indicates that:

$$\begin{aligned} e_d &= \omega L_{ls} f_q \\ e_q &= \omega L_{ls} f_d \end{aligned} \tag{5}$$

where the generalized flows and efforts are indicated with f and e, respectively. Substituting f_d by i_{ds1} and f_q by i_{qs1} in (5) it can be seen that the power absorbed by the lower virtual voltage source is the same that the one delivered by the upper source. i.e. the power delivered/absorved by each one of this sources varies with the selected reference frame but the addition remains always equal to zero.

This analysis can be extended to the rest of the virtual sources. Hence, it is graphically proven what is stated in (Ortega et al., 1993). This is:

"The total power delivered/absorbed by the virtual voltage sources is always zero independently of the selected reference frame".

The complete model in BG is shown in Fig. 3 where all the virtual voltage sources are represented by "**MGY**". Considering that, the power dissipated by the R_{Fe} and R_r is absorbed by the thermal sub-system, the secondary bonds of those **RS**'s enter the thermal sub-system. The voltage sources v_{dr} and v_{qr} in Fig. 1 are zero because it is a squirrel cage rotor. The rest of the electrical components modeled in BG also appear in Fig. 3 where the energetic interaction with the mechanical load (performed with two **MGY**) is also indicated.

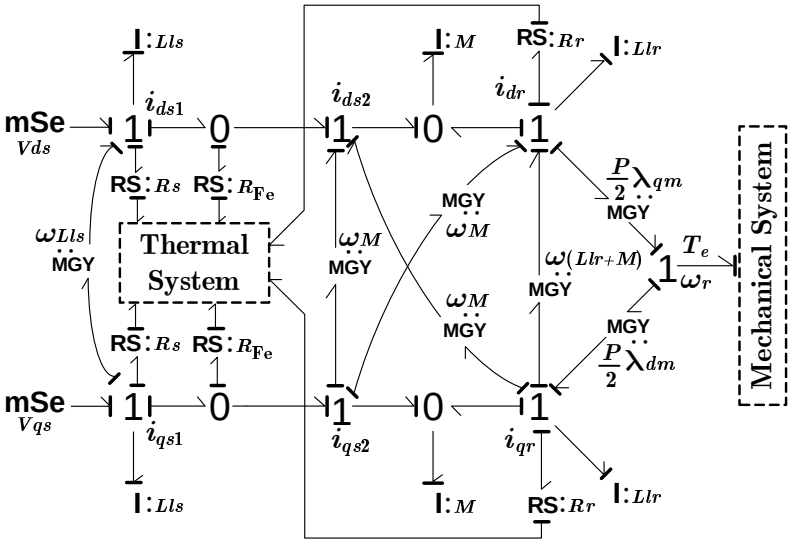

Figure 3: BG representation of the IM in *qd0* variables.

3 MECHANICAL AND THERMAL MODELS

The model displayed in Fig. 3 represents the electric dynamics and manifests the interaction with the thermal and mechanical domain. In order to obtain the complete model, in this section the thermal and mechanical models are presented.

3.1 Thermal Model

The thermal model considers the teeth and slots as independent elements. To keep consistency, the external part of the stator iron is divided into two elements ((1) and (2) in Fig. 4). This array of four elements (shown in Fig. 4) is repeated 36 times which is the number of stator teeth/slots.

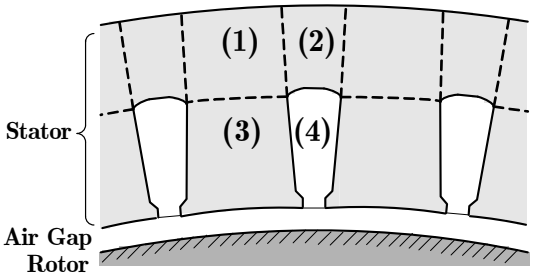

Figure 4: Division of elements in the stator.

Next, the criterion adopted to model the thermal behavior is summarized:

- The external elements interchange heat between them and with the internal elements (3 and 4) by conduction and dissipate heat to the environment.
- The internal elements interchange heat between them and with the external elements by conduction and interact with the rotor through the air-gap.
- The rotor receives the heat dissipated in the rotor resistances, interacts with all the internal elements (through the air-gap) and dissipates heat to the ambient.
- The iron of the stator (elements 1, 2 and 3) receives the heat dissipated in both R_{Fe} that is distributed proportionally to the element's area.
- The 36 slots receive the heat dissipated by the 36 stator resistances (placed in the *abc* frame). The slot where each resistance is placed depends on the way the stator winding is performed (see Fig. 5).
- Thermal radiation is neglected. This criterion is usually adopted when forced ventilation is presented (Boglietti et al., 2003).

3.1.1 Conduction Between Elements

Each of this elements has independent temperature. As consequence of the temperature difference with its neighbor, it interchanges heat by conduction according to the experimental Fourier law:

$$\frac{\partial Q}{\partial t} = -\frac{A}{\rho}\frac{\partial T}{\partial x} \tag{6}$$

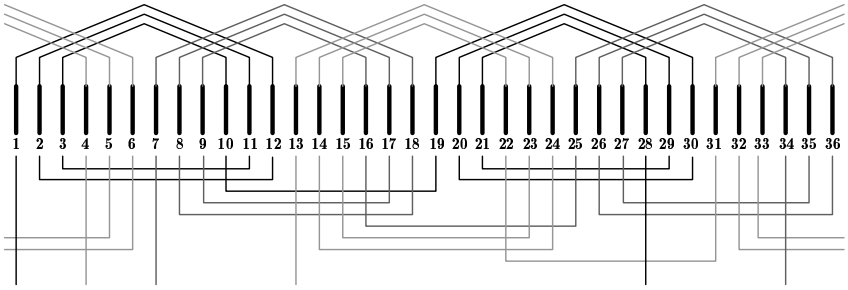

Figure 5: Spatial distribution of stator windings in the stator slots.

The rate of heat transfer ($\partial Q/\partial t$) takes place through the cross-sectional area A; ρ is the thermal resistivity between the elements. $\partial T/\partial x$ is the spatial temperature gradient. In this case:

$$\frac{\partial T}{\partial x} = \frac{\Delta T}{\Delta x} = \frac{(t_i - t_j)}{\Delta x} \tag{7}$$

where $t_{i,j}$ is the element$_{i,j}$ temperature and Δx is the distance between the centre of elements.

3.1.2 Air-gap representation

Given the high relative speed in the air-gap it was proven experimentally in Bastos et al. (1997) that heat transfer by conduction and convection between rotor and stator can be modeled considering the air-gap as a thermal resistance only. Using this virtual thermal resistance both phenomena are included. The identification of the resistance value has to be performed experimentally. Due to the lack of experimental results it was adopted the same value used in the aforementioned work.

3.1.3 Dissipation Toward the Ambient

Under the same hypothesis assumed to model the air-gap, it is possible to model the dissipation toward the ambient as a modulated thermal resistance. In this case the resistivity is a function of the ventilation produced in the motor. Therefore (for a motor without ventilation), it is a function of the vehicle velocity. The element's temperature on the other side of the thermal resistance is the ambient temperature t_{amb}.

3.1.4 Heat Storage

Based on the thermodynamics first law and assuming that neither phase change nor net work occur in the element:

$$Q = \gamma \Delta T \tag{8}$$

where Q is the absorbed heat, γ is the heat capacity and ΔT is the temperature variation produced in the element.

All the sources of entropy plus the incoming/outgoing entropy via conduction conform the total flow of entropy (f). The rate of heat flow ($\partial Q/\partial t$) is obtained by multiplying the total flow of entropy and element temperature (e). Hence, (8) can be re-written in differential form as:

$$f = \frac{\gamma}{e}\frac{de}{dt} \tag{9}$$

This final equation is useful to determine the evolution of the element's temperature when the total flow of entropy and element's initial temperature are known.

3.1.5 Thermal Model in BG

The complete thermal behavior previously described can be modeled in BG (see Fig. 6) using a source of effort to fix t_{amb} and three types of BG elements.

- Thermal conductivity is represented with a thermal resistance "$\mathbf{R_{th}}$" whose relationship between primary and secondary bonds is given by:

$$f_1\, e_1 = \frac{1}{\theta}(e_1 - e_2) \tag{10}$$

$$f_2 e_2 = f_1 e_1 \tag{11}$$

  where the product $f_1\, e_1$ is the rate of heat flow ($\partial Q/\partial t$). Replacing $\theta = \rho\, \Delta x/A$ (thermal resistance), (10) becomes equivalent to (6). To model the effect of ventilation in the dissipation toward the ambient θ varies with V_x according to (Staton et al., 2005):

$$\theta = \theta_0(1 - \beta V_x) \tag{12}$$

  where β represents the reduction in the resistance.

  Eq. (11) states that the outgoing heat from an element is totally transferred to the other.

- The incoming heat by dissipation on the electric resistances is modeled with a modulated resistive source "**RS**". Relationship between primary and secondary bonds is given by:

$$\begin{aligned} e_1 &= R\, f_1 \\ f_2 &= f_1 e_1 / e_2 \end{aligned} \tag{13}$$

  Primary bond (indicated with subscript 1) belongs to the electric domain and has free causality. Secondary bond (subscript 2) enters the thermal model as a source of entropy. For the stator resistances, the value of R is modulated as function of the temperature in the slot where it is placed. Rotor electric resistances vary according to the rotor temperature (t_{rot}). The dependence is given by:

$$R = R_{20}\left[1 + \alpha\,(t_i - 20)\right], \tag{14}$$

  R_{20} is the resistance value at 20°C, t_i is the element's temperature in [°C] and α is the temperature coefficient.

- Heat storage is represented with a thermal capacity $\mathbf{C_{th}}$. It inherits the relationship from electric capacity but in this case the value of the capacity is inversely proportional to element temperature (i.e. $C = \gamma/e$). With this substitution, the relationship becomes equivalent to (9).

The thermal model in BG is finally presented in Fig. 6.

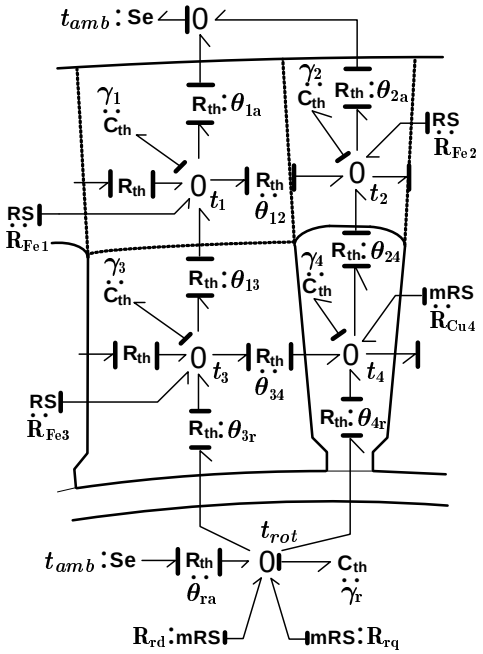

Figure 6: BG representation of the thermal model.

3.2 Mechanical Model

The mechanical model is in correspondence with the prototype under construction by the Applied Electronic Group at the National University of Río Cuarto. The geometry in Fig. 7 responds to the so-called neighborhood electric vehicle.

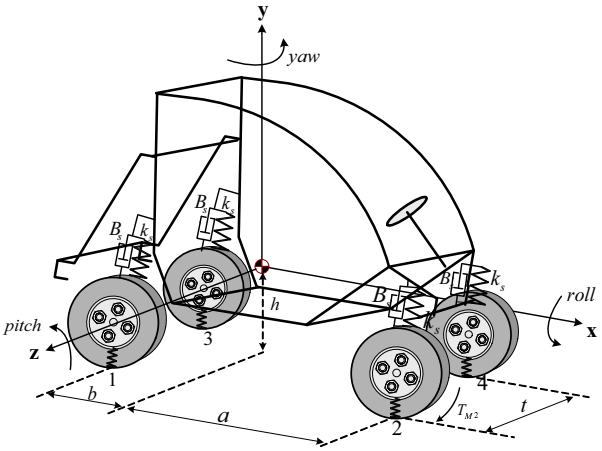

Figure 7: Vehicle model.

The model used in this work does not consider lateral dynamics. Due to the symmetry between left and right side, it is simplified into a half vehicle model with only two wheels (frontal and rear). Given that the vehicle has rear traction, the motor is coupled only to the rear wheel. The rotational dynamics of the rear wheel is given by:

$$I_W \dot{\omega}_W = T_e N - F_r r_W - B_W \omega_W \tag{15}$$

where I_W, ω_W, r_W and B_W are the moment of inertia, velocity, radius and rotational friction coefficient of the wheel, respectively. N is the fixed gear ratio that relates the motor with the

wheel. F_r is the longitudinal force on the patch contact. The dynamics involved in frontal wheel is the same except that $T_e = 0$

The longitudinal dynamics receives the forces produced on the patch contact of rear and frontal wheel (F_r and F_f) and determines de velocity (V_x). The aerodynamic drag force F_{drag} is function of V_x and tends to stop the vehicle. For longitudinal dynamics of half vehicle, the set of equations is:

$$F_r + F_f - F_{drag} = (m_{tot}/2)\,\dot{V}_x \tag{16}$$

$$F_{drag} = \frac{1}{2} C_X\,(A_f/2)\,\rho V_x^2 \tag{17}$$

where m_{tot} and A_f are the total mass and frontal area of the vehicle, respectively. C_X is the aerodynamic coefficient and ρ is the air density.

The physical principles and modeling with BG of the wheel rotational dynamics as well as longitudinal dynamics of the vehicle is presented and discussed in detail in Silva et al. (2008).

4 COMPLETE MODEL

Once the thermal and mechanical models are obtained in section 3, they are integrated together with the electrical model presented in section 2. To obtain the complete model, blocks named "Thermal System" and "Mechanical System" in Fig. 3 are simply replaced by their corresponding BG models.

The energetic interaction between electrical and mechanical parts is performed via two **MGY**. To couple the thermal and electrical sub-systems both R_s are transformed to the *abc* frame and each stator resistance is divided into a series of twelve modulated "RS" whose secondary bond enters the thermal system in the corresponding slot. By inspecting Fig. 4 it can be inferred that there are three iron elements for each slot. Thus, the total power dissipated on each R_{Fe} has to be split into the 108 iron elements. To this purpose, each R_{Fe} is divided into a series of 108 "RS" elements. Their secondary side enters the thermal domain in the stator iron elements and the value of R is proportional to the element area. Both R_r are modulated "RS" with the secondary bond entering the rotor thermal model that is considered as a lumped mass. Finally V_x is fed back to the thermal system (to modulate the ventilation) and ω_W of tractive wheel is used in the electric system (to perform the FOC).

5 SIMULATION RESULTS

The aim is to remark the multidisciplinary feature of the complete model. Along the proposed experiment, the evolution of thermal, electrical and mechanical variables are provided. The outstanding point is that the variables are shown under faulty and non-faulty conditions. The parameters value used to perform the numerical simulation are displayed in table 1.

The experiment consists of a straight line motion with velocity profile determined by **SAE J227a Schedule C** drive cycle. It is repeated 75 times (6000 seconds). During these 75 cycles no fault is included. From that moment, a fault in stator phase "a" is simulated. It was created by duplicating the value of R_a. The complete additional resistance is supposed to be located in the 1^{st} slot. Under this faulty condition, the maneuver is repeated again 75 times. Fig. 8.a shows V_x during two complete cycles. The first one is without fault and the second cycle is performed immediately after the fault occurs. Both profiles are almost equal. This is because the FOC resulted tolerant to that fault, nonetheless the power dissipated by the stator resistances increases considerably (see Fig. 8.b). Also, this figure shows, in the second cycle, an oscillation

in the IM power due to the faulty condition. This oscillation at twice of the supply frequency is a well known effect when a stator asymmetry appears (Legowski et al.)

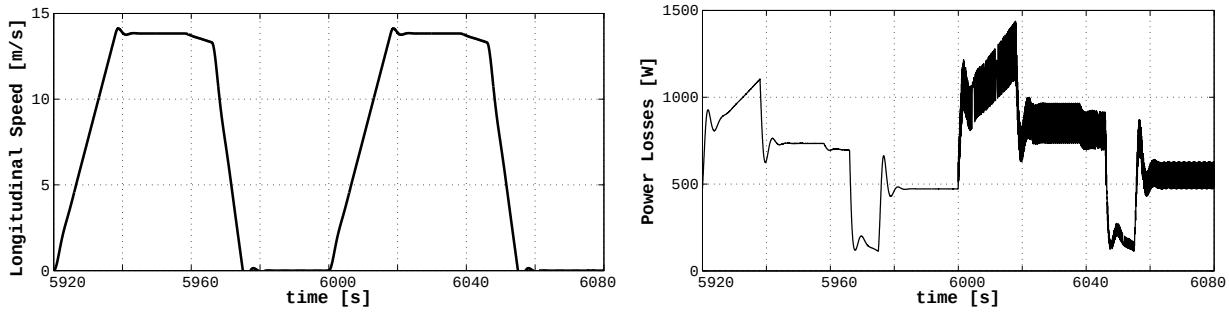

(a) (b)

Figure 8: (a) V_x profile. (b) Power Losses without/with failure.

Fig. 9 shows the temperature evolution of the rotor, the slot where the fault occurs (Cu 1) and the external iron opposed to Cu1 (named Fe 19). In absence of fault, the motor operates in the range of admissible temperatures. Due to the increment in power during the fault, the motor is heated. The most critical part is the slot where the resistance increment took place.

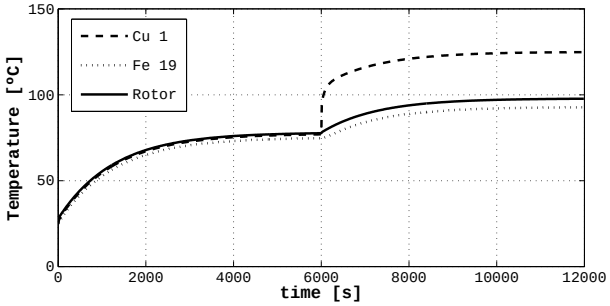

Figure 9: Temperature evolution without/with failure.

6 CONCLUSION

The multi-domain model presented in this work allows to evaluate the impact on the complete system when faults associated to broken rotor bars or stator winding short-circuits occur. This analysis is performed including few modifications in the conventional model of the induction machine in *dq0* variables. In particular, for stator winding short-circuits, the temperature increment in the corresponding slot can be calculated.

In the type of applications tackled in the present work, fault tolerant control strategies are widely used (Lee and Habetler, 2006; Mendes et al., 2008). When this strategies needs to be developed and evaluated, the proposed model becomes a helpful tool.

Future work will be oriented to obtain fault tolerant control strategies and perform their evaluation using the complete model presented in this work.

REFERENCES

Bastos J., Cabreira M., Sadowski N., Arruda S., and Nau S. A thermal analysis of induction motors using a weak coupled modeling. *IEEE Trans. on Magnetics*, 33(2):1714–1717, 1997.

Bellini A., Concari C., Franceschini G., Lorenzani E., Tassoni C., and Toscani A. Thorough understanding and experimental validation of current sideband components in induction machines rotor monitoring. In *IEEE Industrial Electronics, IECON 2006 - 32nd Annual Conference on*, pages 4957–4962. 2006.

Boglietti A., Cavagnino A., and Staton D. Thermal analysis of tefc induction motors. In *Conf. Rec. of the 38th IAS Ann. Meet. Industry Applications Conference, 2003*, volume 2, pages 849–856. 2003.

Cellier F.E. *Continuous System Modeling*. Springer Verlag, New York, 1991.

de la Barrera P.M., Bossio G.R., Solsona J.A., and García G.O. On-line iron loss resistance identification by a state observer for rotor-flux-oriented control of induction motor. *Energy conversion and management*, 49(10):2742–2747, 2008.

Donaire A. *Análisis y síntesis de sistemas no lineales de control en base a propiedades físicas, estructurales y causales de modelos bond graph*. Tesis doctoral, Facultad de Ciencias Exactas, Ingeniería y Agrimensura, Universidad Nacional de Rosario, Rosario, Argentina, 2009.

García G.O. *Controladores Eficientes Para el Accionamiento de Motores de Inducción*. Tesis presentada para grado de dr. en ingeniería, Prog. de Ing. Eléctrica; Coord. Prog de Posgrado en Ing. (COPPE), Univ. Fed. de Río de Janeiro (UFRJ), Río de Janeiro, Brasil, 1994.

García G.O., Mendes Luís J.C., Stephan R.M., and Watanabe E.H. An efficient controller for an adjustable speed induction motor drive. *IEEE Trans. on Industrial Electronics*, 41(5):533–539, 1994.

Junco S. Real and complex power bond graph modeling of the induction motor. In *International Conf. on Bond Graph Modeling and Simulation, ICBGM 1999*, pages 323–328. San Francisco, California, 1999.

Karnopp D. Understanding induction motor state equations using bond graph. In *International Conference on Bond Graph Modeling and Simulation, ICBGM 2003*. Orlando, Florida, USA, 2003.

Karnopp D.C., Margolis D.L., and Rosenberg R.C. *System Dynamics: Modeling And Simulation of Mechatronic Systems*. Willey InterCiences, New York, USA, 2000.

Krause P.C., Wasynczuk O., and Sudhoff S.D. *Analysis of Electric Machinery*. IEEE Press, New York, USA, 1994.

Krishnan R. *Electric Motor Drives: Modeling, Analysis and Control*. Prentice Hall, 2001.

Lamine A. and Levi E. Dynamic induction machine modelling considering the stray load losses. In *Universities Power Engineering Conference, 2004. UPEC 2004. 39th International*, volume 1, pages 582–586. 2004.

Lee Y. and Habetler T.G. A stator turn fault tolerant strategy for induction motor drives in safety critical applications. In *Power Electronics Specialists Conference, 2006. PESC '06. 37th IEEE*, pages 1–7. 2006.

Legowski S.F., Ula A.H.M.S., and Trzynadlowski A.M. Instantaneous power as a medium for the signature analysis of induction motors. *IEEE Trans. on Industry Applications*, 32(4), ????

Levi E. Impact of iron loss on behavior of vector controlled induction machines. *IEEE Trans. on Industry Applications*, 31(6):1287–1296, 1995.

Levi E., Sokola M., Boglietti A., and Pastorelli M. Iron loss in rotor-flux-oriented induction machines: identification, assessment of detuning, and compensation. *IEEE Trans. on Power Electronics*, 11(5):698–709, 1996.

Mendes A.M.S., Lopez-Fernandez X.M., and Marques Cardoso A.J. Thermal performance of a three-phase induction motor under fault tolerant operating strategies. *IEEE Trans. on Power Electronics*, 23(3):1537–1544, 2008.

Ortega R., Canudas C., and Seleme S. Nonlinear control of induction motors: Torque tracking with unknown load disturbance. *IEEE Trans. on Automatic Control*, 38(11):1675–1680, 1993.

Silva L.I., de la Barrera P.M., De Angelo C.H., and García G.O. Análisis, modelado y simulación de la dinámica del motor de inducción usando diagrama de enlaces. In *XIII Reunión de Trabajo en Procesamiento de la Información y Control, RPIC 2009*. Rosario, Argentina, 2009.

Silva L.I., Magallán G.A., De Angelo C.H., and García G.O. Vehicle dynamics using multibond graphs: Four wheel electric vehicle modeling. In *34th Ann. Conf. IEEE Ind. Electronics Society, IECON '08*, pages 2846–2851. Orlando, Florida, 2008.

Staton D., Boglietti A., and Cavagnino A. Solving the more difficult aspects of electric motor thermal analysis in small and medium size industrial induction motors. *IEEE Trans. on Energy Conversion*, 20(3):620–628, 2005.

Tallam R.M., Habetler T.G., and Harley R.G. Transient model for induction machines with stator winding turn faults. *IEEE Trans. on Industry Applications*, 38(3):632–637, 2002.

Table 1: Complete System Parameters

Electrical Domain (rated)		
Power (P_n)	3	[kW]
Line Voltage (V_n)	28	[V]
Current (I_n)	81.56	[A]
Frequency (f_n)	50	[Hz]
Torque (T_e)	19.4	[Nm]
Poles (P)	4	
$R_a = R_b = R_c$	10.476	[mΩ]
R_r	22.231	[mΩ]
R_{Fe}	157	[Ω]
$L_{ls} = L_{lr}$	89.03	[μH]
M	1.21	[mH]
Thermal Domain		
Rotor Heat Capacity (γ_r)	1480	$[J/^\circ C]$
Element 1 Heat Capacity (γ_1)	105.7	$[J/^\circ C]$
Element 2 Heat Capacity (γ_2)	71.1	$[J/^\circ C]$
Element 3 Heat Capacity (γ_3)	178.8	$[J/^\circ C]$
Element 4 Heat Capacity (γ_4)	43.8	$[J/^\circ C]$
Thermal Resistance θ_{12}	0.140	$[^\circ C/W]$
Thermal Resistance θ_{13}	0.097	$[^\circ C/W]$
Thermal Resistance θ_{24}	0.464	$[^\circ C/W]$
Thermal Resistance θ_{34}	0.232	$[^\circ C/W]$
Thermal Resistance θ_{3r}	0.521	$[^\circ C/W]$
Thermal Resistance θ_{4r}	0.975	$[^\circ C/W]$
Thermal Resistance θ_{ra}	1.115	$[^\circ C/W]$
Rated Thermal Resistance $\theta_{1a,0}$	5.188	$[^\circ C/W]$
Rated Thermal Resistance $\theta_{2a,0}$	9.980	$[^\circ C/W]$
Resistance Reduction Coeff. (β)	0.0376	$[s/m]$
Temperarute Coeff. ($\alpha_r = \alpha_s$)	0.00393	$[^\circ C^{-1}]$
Ambient Teperature	25	[°C]
Mechanical Domain		
Wheel Inertia (I_W)	1.95	[kgm^2]
Wheel Radius (r_W)	0.268	[m]
Rotational Friction Coeff. (B_W)	0.023	[Nms]
Fixed Gear Ratio (N)	3	
Vehicle Total Mass (m_{tot})	640	[kg]
Vehicle Frontal Area (A_f)	1.4	$[m^2]$
Aerodynamic Coeff. (C_X)	0.5	
Air Density (ρ)	1.225	$[\frac{kg}{m^3}]$